NANO LETTERS

pubs.acs.org/NanoLett Letter

Maximizing TLR9 Activation in Cancer Immunotherapy with Dual-Adjuvanted Spherical Nucleic Acids

Peiru Chen, Dali Wang, Yuyan Wang, Lei Zhang, Qiwei Wang, Lanxia Liu, Jiahe Li, Xin Sun, Mengqi Ren, Ruoxuan Wang, Yang Fang, Jean J. Zhao, and Ke Zhang*

Cite This: https://doi.org/10.1021/acs.nanolett.2c00723 Read Online

ACCESS | Metrics & More | Article Recommendations | Supporting Information

ABSTRACT: Nucleic-acid-based immune adjuvants have been extensively investigated for the design of cancer vaccines. However, nucleic acids often require the assistance of a carrier system to improve cellular uptake. Yet, such systems are prone to carrier-associated adaptive immunity, leading to difficulties in a multidose treatment regimen. Here, we demonstrate that a spherical nucleic acid (SNA)-based self-adjuvanting system consisting of phosphodiester oligonucleotides and vitamin E can function as a potent anticancer vaccine without a carrier. The two functional modules work synergistically, serving as each other's delivery vector to enhance toll-like receptor 9 activation. The vaccine rapidly enters cells carrying OVA model antigens, which enables efficient activation of adaptive immunity *in vitro* and *in vivo*. In OVA-expressing tumor allograft models, both prophylactic and therapeutic vaccinations significantly retard tumor growth and prolong animal survival. Furthermore, the vaccinations were also able to reduce lung metastasis in a B16F10-OVA model.

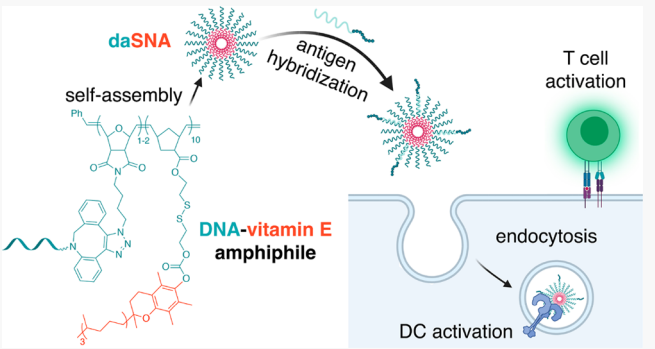

KEYWORDS: *spherical nucleic acids, CpG oligonucleotides, DNA amphiphiles, cancer vaccines*

Nucleic acids represent a key family of adjuvants recognized by several pattern-recognition receptors (PRRs), such as toll-like receptors (TLRs) 3, 7, 8, and 9, retinoic acid inducible gene I (RIG-1), and cyclic-GMP-AMP synthase (cGAS).[1−4] For immunoregulatory applications, however, nucleic acids face significant cellular and *in vivo* pharmacological barriers, including poor cell uptake, nuclease instability, and rapid renal clearance. Thus, it is often more appealing to consider alternative activation strategies such as synthetic small-molecule agonists or antagonists.[5−9] While many such ligands are in development, few have reached regulatory approval.[10,11] In addition, spatiotemporally controlled codelivery with soluble antigens, which suffer from fast clearance, poor lymph node (LN) draining/retention, and inefficient colocalization, remains a challenge.[12,13] To codeliver the antigens with a ligand for nucleic-acid-related PRRs (either natural or synthetic), a cocarrier system is often required.[14−19] However, such a cocarrier is prone to anticarrier adaptive immunity in a stimulated immune system.[20] Thus, it is ideal if the adjuvant and the antigen form a self-delivering construct that can reach the target tissue and cellular organelle/cytoplasm without additional immunogenic epitopes that can lead to unwanted activation of adaptive immunity.[21,22] While it is still possible to generate antinucleic acid antibodies, it has been reported that immunogenicity is phosphorothioate backbone specific.[23]

Herein, we have designed a cancer vaccine consisting of a spherical nucleic acid (SNA) core hybridized to an antigen−oligonucleotide conjugate (Figure 1A). The dual-adjuvanted SNA (daSNA) is assembled from a DNA amphiphile having a CpG-rich oligonucleotide hydrophilic segment and a vitamin E (VE) containing hydrophobic segment; the latter can be released bioreductively (Figure S1C).[24,25] Not only does the VE component serve as the hydrophobic driving force for SNA formation but also the released VE can also work synergically with CpG DNA to amplify immune responses.[26,27] Although no carrier is involved, the daSNA vaccine undergoes rapid cellular uptake into endocytic compartments, where TLR9 is predominantly located. Activation of the TLR9-MyD88 pathway leads to dendritic cell (DC) activation, upregulation of proinflammatory cytokines, sequential antigen-specific T cell proliferation, and ultimately strong antigen-specific immune responses.[28,29] In addition, the daSNA vaccine was retained in the draining lymph node (dLN) to a much higher extent in comparison to a physical mixture of the antigen/adjuvant. Both

Received: February 22, 2022
Revised: April 29, 2022

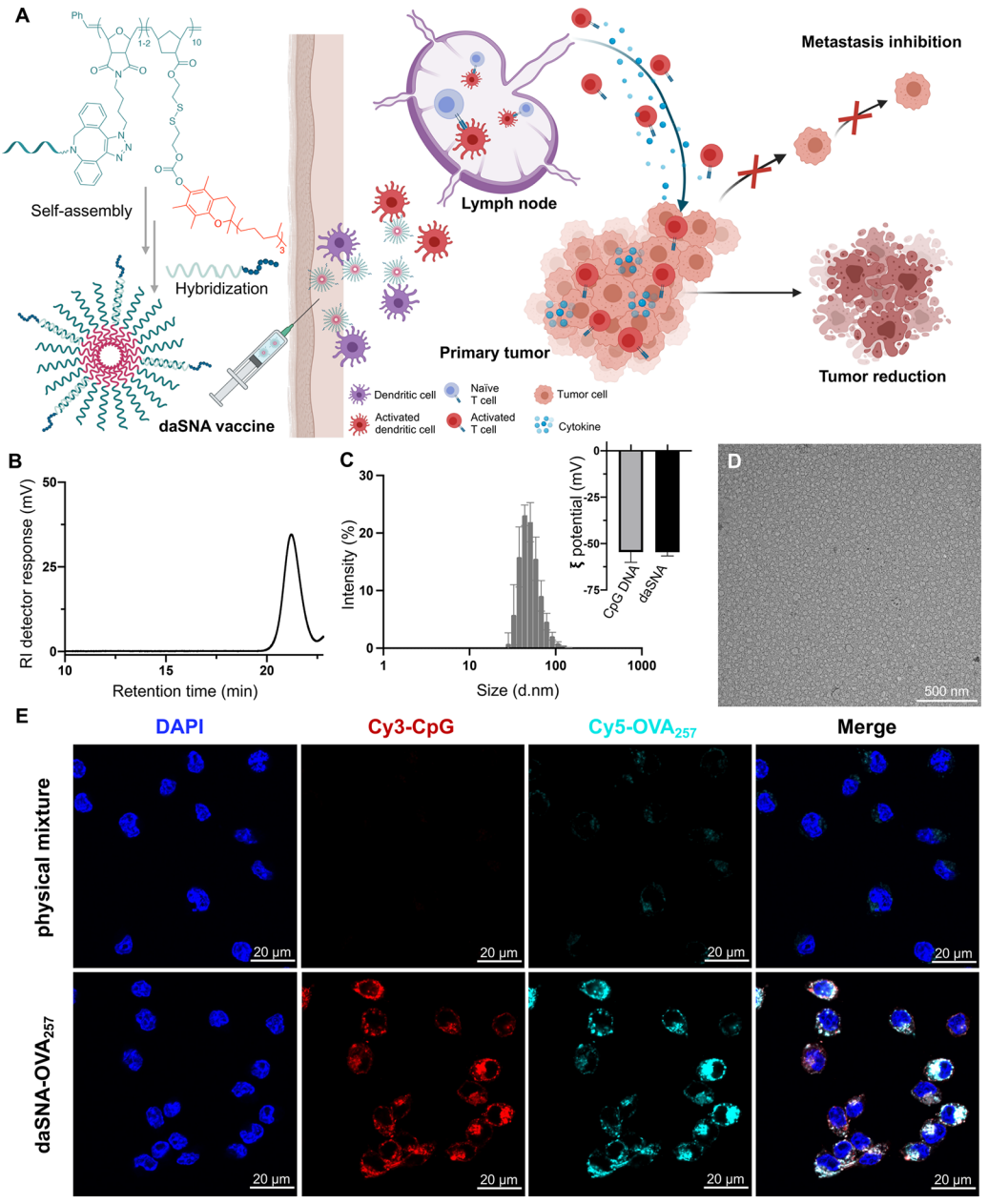

Figure 1. Mechanism of action and physical characterization of the daSNA vaccine. (A) Chemical structure and schematic representation of the daSNA vaccine and the mode of action for the antigen-specific antitumor effect *in vivo*, created with BioRender.com. (B) DMF GPC of the poly(VE)-Br precursor for the daSNA vaccine. (C) DLS number-average size distribution of poly(VE)-CpG daSNA. Insert: ζ potential (mV) of the daSNA in comparison to that of free CpG DNA in 1× PBS buffer. (D) TEM micrograph of the poly(VE)-CpG daSNA, negatively stained with 2% uranyl acetate. (E) Confocal microscopy of DC2.4 cells treated with test agents, showing significantly enhanced cellular uptake of antigen/adjuvant and their colocalization for the daSNA vaccine in comparison with a free mixture of the constituent components.

prophylactic and therapeutic application of the vaccine against cancer cells expressing ovalbumin (OVA, model antigen) in mouse allograft tumor models resulted in decidedly prolonged animal survival. In addition, the vaccination substantially reduced lung metastasis. Consisting almost entirely of naturally occurring compounds (DNA/VE > 85% by molecular weight), the daSNA vaccine represents a powerful vaccinology approach for developing potent natural agonists for nucleic-acid-associated PRRs while eliminating the safety and immunological concerns over an added cocarrier system.

Design and Material Preparation. To synthesize the poly(VE) segment, α-tocopherol (a common VE form) was linked to a polymerizable monomer via a bioreductively cleavable linker. α-Tocopherol was sequentially reacted with triphosgene and 2-hydroxyethyl disulfide modified norbornene (compound **1**, Figure S1A) to yield the norbornenyl VE monomer (N-SS-VE, Figure S1A). For robust micelle formation, a degree of polymerization of 10 was targeted. Sequential copolymerization of N-SS-VE monomer (10 equiv) with an oxanorbornene bromide (N-Br, 2 equiv) gives a narrowly dispersed block copolymer (PDI = 1.13, M_n = 4.3 kDa; Figure 1B) with a high yield (~96%). Substitution of the bromides with azides gives the hydrophobic portion of the amphiphile, poly(VE)-N_3, which was then conjugated to a 5′-dibenzocyclooctyne-modified ODN1826 (a CpG-rich oligonucleotide, henceforward abbreviated as "CpG") via copper-

https://doi.org/10.1021/acs.nanolett.2c00723
Nano Lett. XXXX, XXX, XXX−XXX

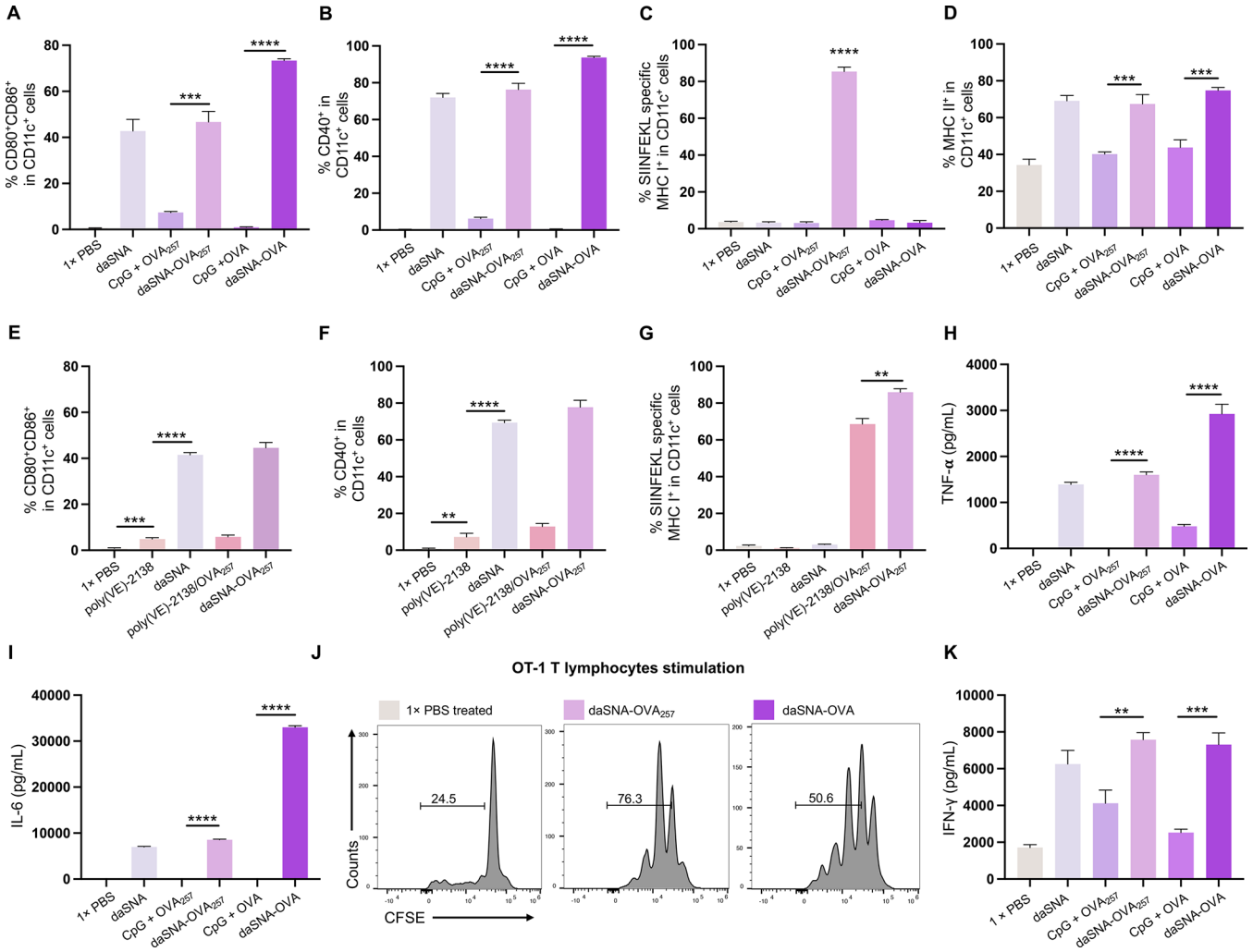

Figure 2. Stimulation of BMDCs and proliferation of the antigen-specific T lymphocytes *in vitro*. (A–D) $CD80^+CD86^+$, $CD40^+$, SIINFEKL-specific MHC I^+, and MHC II^+ DC populations ($CD11c^+$) after treatment with daSNA vaccines and the corresponding physical mixtures as negative controls. (E–G) $CD80^+CD86^+$, $CD40^+$, and SIINFEKL-specific MHC I^+ DC populations ($CD11c^+$) after treatment with daSNA vaccines and negative control SNA containing a nonagonist for TLR9 (GpC instead of GpG, ODN2138). (H, I) TNF-α and IL-6 levels in the extracellular supernatant after treatment with daSNA vaccines and controls. (J) CFSE dilutions of $CD8^+$ lymphocytes derived from OT-1 mice after direct stimulation with daSNA vaccines and controls. (K) IFN-γ levels in the supernatant of lymphatic cells derived from OT-1 mice after direct stimulation with daSNA vaccines and controls.

free click chemistry to yield the final DNA amphiphile, poly(VE)-CpG (Figure S1B). The amphiphile spontaneously forms micellar structures in an aqueous buffer (1× PBS), as evidenced by a narrow, more slowly migrating band in agarose electrophoresis (2%) in comparison to free CpG (Figure S2). Transmission electron microscopy (TEM; Figure 1D) shows that the self-assembly yields uniform daSNAs with an average dry-state diameter of 42.6 ± 6.0 nm, which is corroborated by dynamic light scattering (DLS) measurements (number-average hydrodynamic diameter 51.7 ± 3.6 nm; Figure 1C). This size is within the appropriate range for dLN targeting, where 10–100 nm particles have been shown to exhibit the best dLN localization.[30] In addition, the daSNA shows a ζ potential of −54.6 ± 5.6 mV, which is similar to that of the free CpG DNA (Figure 1C).

Next, model antigens (OVA protein or the peptidyl epitope, SIINFEKL) were covalently functionalized with the complementary DNA (cDNA) of the CpG sequence. The conjugate is to be used to decorate the daSNA core with antigens through hybridization. Once the daSNA vaccine undergoes endocytosis, the labile ester or disulfide linkages can be enzymatically or bioreductively cleaved, so that antigens can be presented via major histocompatibility complex (MHC) I or II.[31,32] For OVA modification, a succinimidyl 4-(*N*-maleimidomethyl)-cyclohexane-1-carboxylate linker was used to derivatize the exposed amino groups with a maleimide group, which enabled subsequent conjugation with thiol-modified cDNA (Figure S3B–D). For SIINFEKL (later denoted "OVA_{257}"), a cystine residue was appended at the C terminus, which was sequentially reacted with 2,2′-dipyridyl disulfide and thiol-modified cDNA via a thiol-exchange reaction (Figure S3A,E). The successful syntheses were confirmed by matrix-assisted desorption–ionization mass spectrometry (MALDI-TOF), gel permeation chromatography (GPC), reversed-phase HPLC, and gel electrophoresis (Figure S4). Hybridization of purified cDNA–antigen conjugates to the SNA (1 mol:0.2 mol CpG:cDNA) yields the final daSNA vaccines (daSNA-OVA and daSNA-OVA_{257}). Hybridization was confirmed by gel electrophoresis, showing that the antigen component (Cy5 or FITC) colocalizes with the Cy3-labeled SNA (Figure S5A) and

https://doi.org/10.1021/acs.nanolett.2c00723
Nano Lett. XXXX, XXX, XXX–XXX

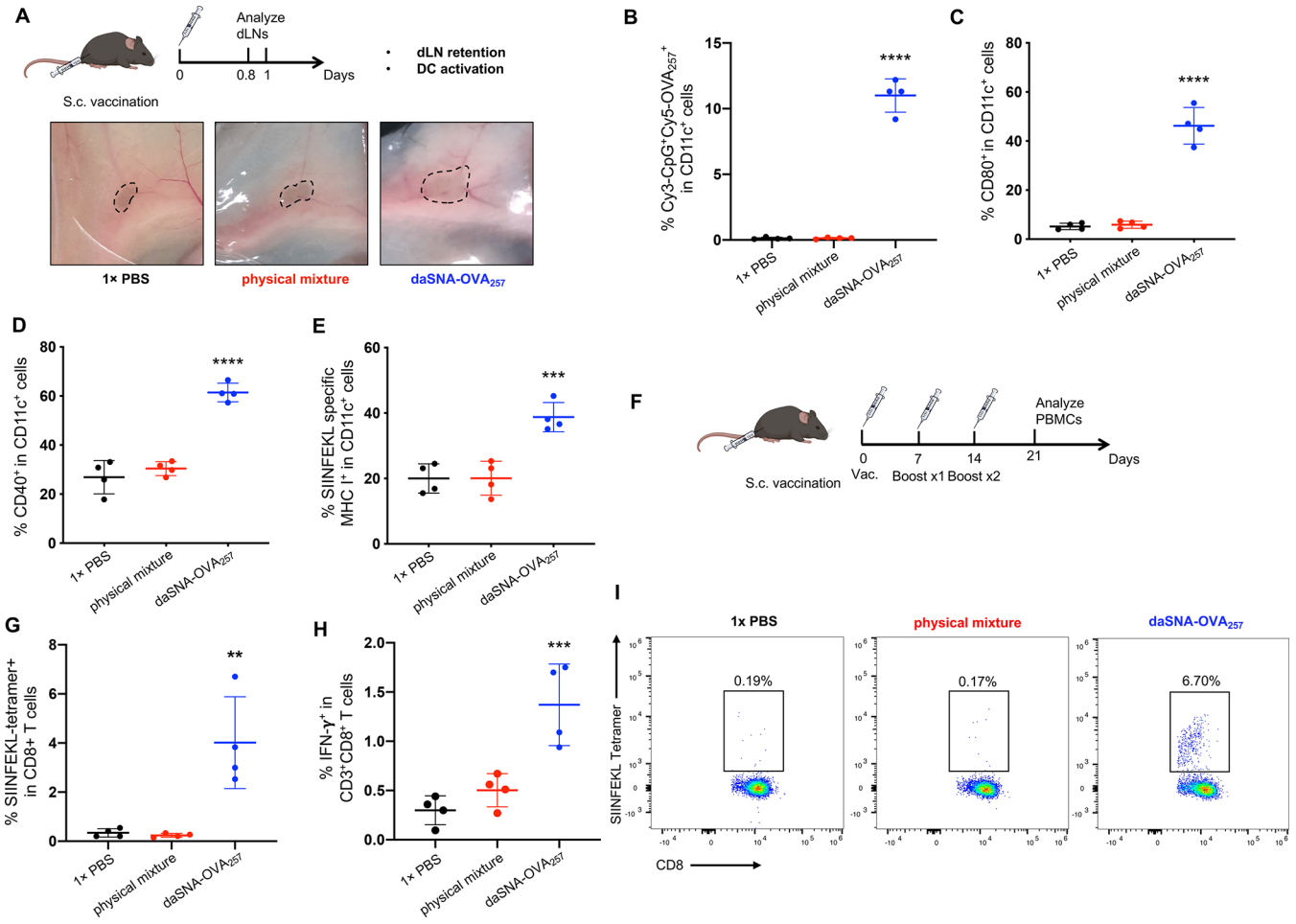

Figure 3. daSNA-OVA$_{257}$ promotes DC activation and lymph node retention and primes the antigen-specific T cells *in vivo*. (A) Representative photographs of mouse dLNs 20 h after initial s.c. vaccination. (B) Flow cytometry analysis of double-positive (antigen$^+$adjuvant$^+$) DCs 24 h after initial s.c. vaccination. (C−E) *In vivo* DC costimulatory markers (CD80 and CD40) and antigen presentation (SIINFEKL-MHC I) 20 h after initial s.c. vaccination. (F) Schedule for vaccinations and analysis of PBMCs. (G) Flow cytometry analysis of SIINFEKL-specific cytotoxic T cell population (SIINFEKL-tetramer$^+$CD8$^+$) in PBMCs. (H) Flow cytometry analysis of IFN-γ secreting cytotoxic T cells in PBMCs. (I) Representative flow cytometry density plot of SIINFEKL-specific cytotoxic T cells in PBMCs after vaccination with daSNA-OVA$_{257}$ and controls.

that the bands corresponding to free cDNA−antigens have disappeared after hybridization (Figure S5B).

SNA-Assisted Intracellular Delivery of Antigens. Key factors for inducing strong antigen-specific immune responses include high levels of cellular uptake and the simultaneous codelivery of antigens/adjuvants into the same APC.[33,34] To investigate the uptake of the daSNA, murine DCs (DC2.4) were treated with dual-fluorescently-labeled particles and analyzed by flow cytometry. In comparison to DC2.4 treated with a physical mixture of antigens and free CpG oligonucleotide, cells treated with daSNA exhibited markedly increased mean fluorescence intensities (MFIs) for both the CpG and the antigen (Figure S6). The daSNA structure increased the uptake of CpG by 23-fold, while the uptakes of OVA/OVA$_{257}$ were both enhanced by 6-fold (at 1 μM CpG). The elevated uptake is likely due to caveolae/lipid-raft-dependent endocytosis, previously observed for SNAs consisting of a gold nanoparticle core.[35] The flow cytometry results were corroborated by confocal microscopy, which shows stronger fluorescent signals from both CpG and antigen channels for DC2.4 treated with the daSNA vaccines relative to those treated with the corresponding physical mixture at identical concentrations (Figures 1E and Figure S7A). The signals appear as colocalized, punctate patterns, which is indicative of entrapment of intact particles within endocytic compartments.

DC Activation and Antigen-Specific T Cell Proliferation *In Vitro*. We next investigated APC activation stimulated by the daSNA vaccines *in vitro*. Mouse bone marrow derived DCs (BMDCs) were incubated with either a daSNA vaccine or its corresponding physical mixture at identical antigen/adjuvant concentrations for 18 h before a flow cytometry analysis. Examining costimulatory markers related to BMDC-maturation (CD86$^+$, CD80$^+$, and CD40$^+$), daSNA vaccines showed significant BMDC maturation over both the vehicle (Figure 2A,B) and the physical mixture. We attribute the BMDC maturation to the daSNA core because an antigen-free SNA was also able to induce similar BMDC maturation. The cell supernatants were also collected for an enzyme-linked immunosorbent assay (ELISA) to test cytokines expressed by BMDCs (TNF-α, IL-12p70, and IL-6). Consistently, strong cytokine expressions were induced by daSNA (Figure 2H,I and Figure S8B). Molecular VE has been shown to work synergistically with CpG.[36] To test the contribution of VE, a non-TLR9 agonist sequence (ODN2138) with altered CG position was used to construct

https://doi.org/10.1021/acs.nanolett.2c00723
Nano Lett. XXXX, XXX, XXX−XXX

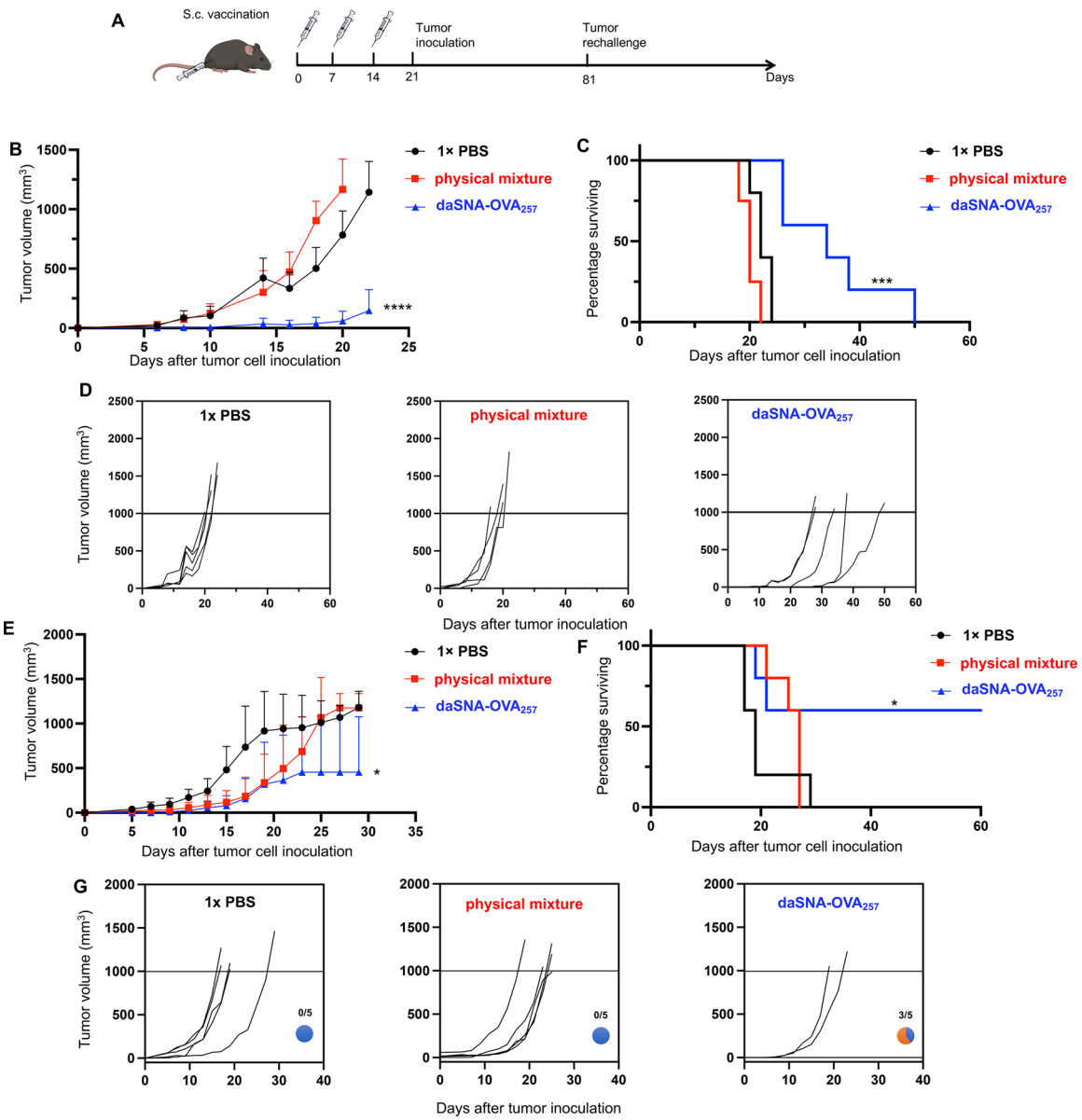

Figure 4. daSNA-OVA_{257} vaccination provides prophylaxis against tumor growth. (A) Vaccination and tumor inoculation schedules. (B) Average tumor growth curve after inoculation with B16F10-OVA cells (tumor volume = $(\text{width})^2 \times \text{length} \times 0.5$). (C) Kaplan−Meier animal survival analysis of mice inoculated with B16F10-OVA cells. (D) Individual tumor growth curves of mice receiving B16F10-OVA cells. (E) Average tumor growth curve after inoculation with MC38-OVA cells. (F) Kaplan−Meier animal survival analysis of mice with inoculated with MC38-OVA cells. (G) Individual tumor growth curves of mice receiving MC38-OVA cells.

a negative control SNA. Flow cytometry showed that the poly(VE)-2138-based SNA induced a lower (but still statistically significant) level of DC maturation relative to the vehicle (Figure 2E,F). The contribution of VE was more pronounced when the BMDC antigen cross-presentation levels were examined (SIINFEKL-specific MHC I). It was found that BMDCs treated with the poly(VE)-2138 SNA and daSNA (both with OVA_{257}) showed comparable levels of antigen presentation (with 85.40% and 68.63% $SIINFEKL^+CD11c^+$ cell populations, respectively; Figure 2G). For MHC II presentation, the percentage of MHC II^+CD11c^+ DCs was significantly boosted for the daSNA vaccines in comparison to the physical mixtures (Figure 2D), which is in line with BMDC maturation results. Similarly, replacing the CpG sequence with ODN2138 caused a noticeable decrease but not complete loss of MHC II^+CD11c^+ DCs. These results suggest that the synergy between CpG and VE extends beyond enhanced endocytosis (Figure S8A).

The ability of the daSNA vaccines to raise antigen-specific T cell response was also tested *in vitro* using lymphatic cells derived from transgenic OT-1 mice, whose $CD8^+$ T lymphocytes have an immune memory toward OVA_{257}. Carboxyfluorescein succinimidyl ester (CFSE) labeled OT-1 lymphatic cells were incubated with the daSNA vaccines or controls for 48 h and analyzed by flow cytometry. Both vaccines induced the proliferation of OVA_{257}-specific $CD8^+$ T cells, as evidenced by fluorescence dilution. Notably, the daSNA-OVA_{257}-treated lymphatic cells exhibited similar OVA_{257}-specific T lymphocyte proliferation in comparison to free OVA_{257} (Figure 2J and Figure S8C), suggesting that OVA_{257} tethered to the daSNA surface can be recognized by antigen-specific $CD8^+$ T lymphocytes as efficiently as free

https://doi.org/10.1021/acs.nanolett.2c00723
Nano Lett. XXXX, XXX, XXX−XXX

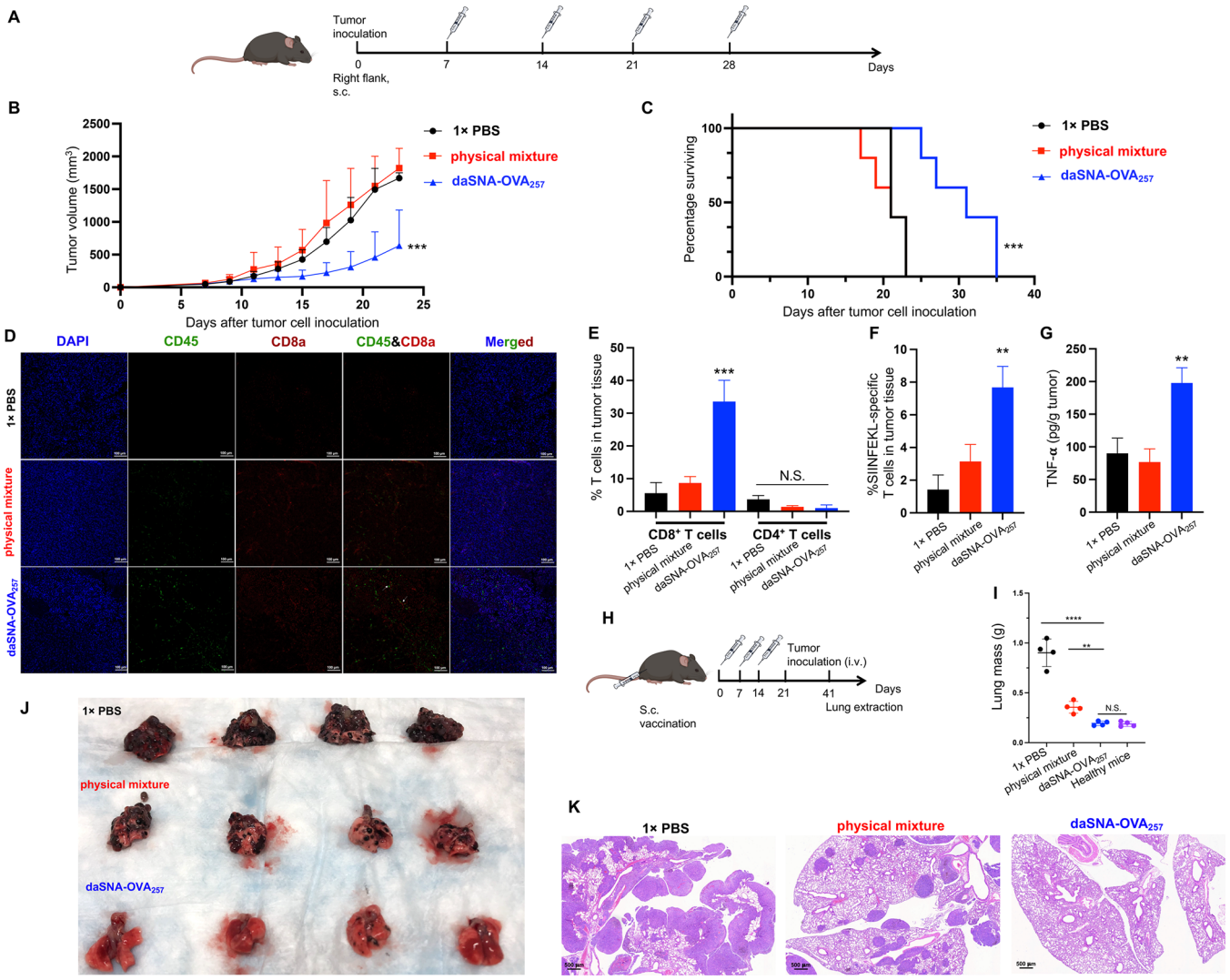

Figure 5. Therapeutic efficacy, mechanistic study, and lung metastasis prevention of the daSNA treatment. (A) Schedule for tumor inoculation (B16F10-OVA cell line) and therapeutic dosing. (B) Average tumor growth curve after inoculation. (C) Kaplan−Meier animal survival analysis. (D) Representative confocal microscopy images of the $CD45^+CD8^+$ T cells in the tumor microenvironment. (E) Prevalence of $CD45^+CD3^+CD8^+$ and $CD45^+CD3^+CD4^+$ T cells in the tumor microenvironment. (F) Prevalence of SIINFEKL-tetramer$^+CD8^+$ T cells in the tumor microenvironment. (G) TNF-α expression levels in the tumor tissues, normalized to the tumor weight. (H) Schedule for vaccination, establishment of a lung metastasis model (B16F10-OVA/GFP), and lung extraction. (I) Lung mass measured 20 days after tumor inoculation. (J) Photographs of mouse lungs extracted 20 days after tumor inoculation. (K) H&E staining of the vaccinated mouse lungs collected after tumor inoculation. The nuclei-rich regions represent tumor metastases.

OVA_{257}. In addition, the IFN-γ expression levels in the supernatant of the cell culture after 72 h incubation (Figure 2K) were significantly higher for the daSNA vaccines in comparison to their corresponding physical mixtures. Given the robust performance of daSNA-OVA_{257} for stimulating DC maturation, antigen cross-presentation, and antigen-specific cytotoxic T cell proliferation, this particle was selected for subsequent *in vivo* studies.

Targeting DCs *In Vivo* and Antigen-Specific Cytotoxic T Cell Response. In lymphatic circulation, lymph nodes (LNs) are the major sites where immune cells reside. Thus, efficient trafficking to LNs is essential to generate a strong immune response. To investigate LN retention of daSNA-OVA_{257} *in vivo*, daSNA- OVA_{257} or the physical mixture (CpG-Cy3 and OVA_{257}-Cy5) were subcutaneously (s.c.) injected in the right flank of C57BL/6 mice. After 24 h, the inguinal LNs approximate to the injection site were extracted and the lymphatic cells were analyzed by flow cytometry. Remarkably, the daSNA-OVA_{257} resulted in nearly a 100-fold higher double-positive ($CpG\text{-}Cy3^+OVA_{257}\text{-}Cy5^+$) DC population ($CD11c^+$) in comparison to the physical mixture (Figure 3B), indicating that the daSNA-OVA_{257} significantly increased trafficking of DCs into the LNs and the retention of the antigen/adjuvants in LNs. In addition, the extracted LNs are visibly enlarged for mice dosed with daSNA-OVA_{257} in comparison with the vehicle- or the physical-mixture-treated mice (Figure 3A), which indicates increased cellularity. Through flow cytometry, we identified substantially increased populations of matured DCs ($CD80^+$ and $CD40^+$ in $CD11c^+$ DCs) as well as an improved $CD11c^+$ DC population presenting a SIINFEKL-specific MHC I marker (Figure 3C−E). These observations demonstrate that daSNA-OVA_{257} strongly stimulates DC maturation and antigen presentation *in vivo*, which is essential for antigen-specific immunity.

https://doi.org/10.1021/acs.nanolett.2c00723
Nano Lett. XXXX, XXX, XXX−XXX

To investigate the level of antigen-specific T cell response induced by vaccination, we injected daSNA-OVA_{257}, a physical mixture, or a vehicle s.c. in the right flank of C57BL/6 mice weekly for a total of three injections. On day 21, the peripheral blood from immunized mice was collected, and the percentage of antigen-specific T cells among peripheral blood mononuclear cells (PBMCs) was analyzed by flow cytometry (Figure 3F). While immunization with the physical mixture of CpG/OVA_{257} produced no elevation in OVA_{257}-specific cytotoxic T cell population (OVA_{257}-tetramer$^+$CD8$^+$) in comparison to vehicle treatment, mice receiving daSNA-OVA_{257} showed a considerably increased OVA_{257}-specific T cell population (~10-fold, Figure 3G,I). The population of IFN-γ-secreting cytotoxic T cells (IFN-γ^+CD8$^+$CD3) was also similarly increased by the immunization (Figure 3H). Collectively, these results strongly suggest that daSNA-OVA_{257} can stimulate the antigen-specific T cell response *in vivo* and point to potent antitumor activity.

Prophylactic Inhibition of Tumor Growth. We next examined whether the vaccination leads to prophylactic protection against OVA-expressing tumor cells in mice. C57BL/6 mice were vaccinated with daSNA-OVA_{257}, its constituent mixture, or 1× PBS for a total of three times with 1 week intervals. Seven days after the final vaccination, one million B16F10-OVA (melanoma) or MC38-OVA (colon carcinoma) cells were injected s.c. in the right flank (Figure 4A). For the highly aggressive B16F10-OVA model, daSNA-OVA_{257} vaccination produced decidedly retarded tumor growth, averaging 147 mm^3 at 22 days in comparison to 1166 mm^3 for the physical mixture, which leads to longer animal survival (~34 vs 20 days for the physical mixture) (Figure 4B−D and Figure S10). The physical-mixture-treated group exhibited no statistical difference from the vehicle group. For the MC38-OVA model, all mice receiving the physical mixture or PBS reached the end point (tumor size ≥1000 mm^3) within 30 days (Figure 4E−G). In contrast, ~60% of mice receiving the daSNA-OVA_{257} vaccination were tumor-free for 60 days. The immunological memory raised by the vaccination was tested by rechallenging the remaining mice that survived the initial MC38-OVA tumor inoculation with another million MC38-OVA tumor cells in the opposite flank on day 60. In comparison to same-aged naïve C57BL/6 mice, which reached the end point within 20 days, the vaccinated mice showed slower tumor induction and prolonged survival (25 days) (Figure S11A,B).

The mechanism of long-term immunological protection was studied by comparing the memory cytotoxic T cell (CD8$^+$) populations (effective memory T cells (T_{EM}) CD62L$^-$CD44$^+$ and central memory T cells (T_{CM})] CD62L$^+$CD44$^+$ between the surviving and naïve mice. Sixty days after the initial inoculation of MC38-OVA cells, PBMCs were extracted from the surviving mice and same-aged naïve mice, and the percentages of T_{EM} and T_{CM} were analyzed. In comparison to the naïve mice, the surviving mice showed an ~2.3× increase in the T_{EM} population, while T_{CM} exhibited no significant difference (Figure S11C,D). Collectively, these data indicate that daSNA-OVA_{257} provides effective immune stimulation, leading to prophylactic protection and long-term immunological memory.

Therapeutic Suppression of Tumor Growth and Inhibition of Lung Metastasis. To investigate the therapeutic efficacy of daSNA-OVA_{257} treatment, we established B16F10-OVA allografts in the right flank of C57BL/6 mice (Figure 5A). Once the tumor size reached 50 mm^3, treatments with daSNA-OVA_{257} or its physical mixture were carried out by s.c. injection with weekly intervals in the right flank. For the PBS- and physical-mixture-treated groups, all animals reached the end point within 21 days (Figure 5B,C and Figure S12). In contrast, mice receiving daSNA-OVA_{257} exhibited evidently slower tumor growth and prolonged survival (~31 days).

To study the therapeutic mechanism, B16F10-OVA allografts were allowed to grow to a size of 200 mm^3 in the right flank of C57BL/6 mice. Thereafter, daSNA-OVA_{257} or controls were injected s.c. twice (1 week apart). Three days after the second treatment, the tumor tissues were extracted for tumor microenvironment (TME) analysis. The percentage of CD3$^+$CD8$^+$ T cells within the TME of daSNA-OVA_{257}-treated mice was greatly elevated (~6-fold) in comparison to mice receiving either the physical mixture or the control, as determined by confocal microscopy (Figure 5D) and flow cytometry (Figure 5E). The population of antigen-specific cytotoxic T cells (OVA_{257}-tetramer$^+$CD8$^+$) was also significantly increased (~2-fold) (Figure 5F). In addition, an elevation of tumor necrosis factor α expression (Figure 5G) within the tumor tissues was observed, which may have contributed to the overall therapeutic response. Differences in CD3$^+$CD4$^+$ T populations among treatment groups were not evident.

Tumor metastasis is a major threat after the primary tumor has been treated. Thus, we tested the ability of daSNA-OVA_{257} vaccination to prophylactically prevent lung metastasis. C57BL/6 mice received three doses of daSNA-OVA_{257} or the physical mixture every 7 days. On day 21, B16F10-OVA cells (0.5 million) were injected intravenously in the tail vein (Figure 5H). Twenty days after the inoculation, lungs were harvested to evaluate mass, tumor nodule abundance, and histological features. While lungs from mice injected with the PBS control exhibited a large number of overlapping tumor nodules (as evidenced by the dark melanin pigmentation, Figure 5J), the daSNA-OVA_{257} vaccine induced a strong antimetastatic effect in mice with few to no nodules. Interestingly, the physical mixture was also able to induce some antimetastatic effect, but to a much lesser degree in comparison to daSNA-OVA_{257}. Lung weight measurement paints a similar picture: PBS- and physical-mixture-treated mice showed markedly increased lung masses (0.90 ± 0.14 and 0.36 ± 0.06 g, respectively), while mice vaccinated with daSNA-OVA_{257} exhibited a lung mass similar to that of healthy mice (0.19 ± 0.02 and 0.19 ± 0.03 g, respectively) (Figure 5I). Hematoxylin and eosin staining of the lungs of daSNA-OVA_{257}-vaccinated mice showed no significant tumor nodules or histological variations from a normal lung, while both control groups exhibited an abundance of nodules (nuclei-rich, deeper-stained regions) (Figure 5K and Figure S13). Taken together, these results indicate that daSNA-OVA_{257} drastically retards the progression of the highly aggressive melanoma tumor model and reduces the likelihood of lung metastasis.

With regard to the safety of the daSNA-OVA_{257}, no apparent toxicity was observed in BMDCs extracted from C57BL/6 mice and in DC2.4 cells up to 2 μM (nucleic acid basis), as determined by a 3-(4,5-dimethylthiazol-2-yl)-2,5-diphenyltetrazolium bromide (MTT) cytotoxicity assay (Figure S14). In addition, mice treated with daSNA-OVA_{257} did not exhibit evidence of acute sepsis or septic shock, such as hypotension and hypothermia, and no obvious changes in behavior (refusal

https://doi.org/10.1021/acs.nanolett.2c00723
Nano Lett. XXXX, XXX, XXX−XXX

to eat, startle response, etc.) were observed. With repeated vaccinations/treatments, daSNA-OVA_{257} induced no significant weight changes (Figure S15A–C) or noticeable damage to major organs (Figure S16). Thus, daSNA-OVA_{257} appears to exhibit an acceptable safety profile while sufficiently stimulating the immune system for a potent anticancer response.

In summary, we have developed a nanoparticle vaccine based on an CpG DNA-poly(VE) amphiphile termed daSNA, whose surface consists almost entirely of antigens and adjuvants. The core VE component allows the conjugate to assemble into a dense, spherical form, enabling otherwise non-cell-penetrating CpG to undergo rapid endocytosis. Thus, the daSNA bypasses the need for potentially toxic and/or immunogenic synthetic vectors and transforms otherwise difficult pharmaceutical properties of the CpG and VE into beneficial properties, which allow their efficient codelivery. The construct exhibits excellent dLN targeting and retention, which results in improved *in vivo* immune system stimulation. A noteworthy advantage of the daSNA vaccine is that the constituent natural phosphodiester ligand for TLR9 (CpG) can be metabolized, which reduces the risk of persistent or uncontrolled immune system stimulation by nondegradable synthetic analogues and toxicity concerns associated with chemical analogues. When the results are taken ogether, the daSNA vaccine reported here represents a safe, simple, and effective approach to convert natural nucleic acids into high-performance adjuvants, which paves the way for carrier-free vaccine designs for cancer and other immunoregulatory needs.

■ ASSOCIATED CONTENT

Supporting Information

The Supporting Information is available free of charge at https://pubs.acs.org/doi/10.1021/acs.nanolett.2c00723.

Materials, instrumentation, methods, synthetic procedures, NMR data, additional material characterization (MALDI-TOF MS, gel electrophoresis, SEC), additional cellular uptake (flow cytometry and confocal microscopy), additional *in vitro* BMDC and OT1 immunoactivation results, additional *in vivo* LN DC activation ($MHC\ II^+$), additional *in vivo* antitumor results, *in vitro* and *in vivo* safety results, flow cytometry gating, DNA sequence information, and supporting references (PDF)

■ AUTHOR INFORMATION

Corresponding Author

Ke Zhang − *Departments of Chemistry and Chemical Biology, Chemical Engineering, and Bioengineering, Northeastern University, Boston, Massachusetts 02115, United States;* orcid.org/0000-0002-8142-6702; Email: k.zhang@northeastern.edu

Authors

Peiru Chen − *Departments of Chemistry and Chemical Biology, Chemical Engineering, and Bioengineering, Northeastern University, Boston, Massachusetts 02115, United States*

Dali Wang − *Departments of Chemistry and Chemical Biology, Chemical Engineering, and Bioengineering, Northeastern University, Boston, Massachusetts 02115, United States*

Yuyan Wang − *Departments of Chemistry and Chemical Biology, Chemical Engineering, and Bioengineering, Northeastern University, Boston, Massachusetts 02115, United States*

Lei Zhang − *Departments of Chemistry and Chemical Biology, Chemical Engineering, and Bioengineering, Northeastern University, Boston, Massachusetts 02115, United States*

Qiwei Wang − *Department of Cancer Biology, Dana-Farber Cancer Institute, Boston, Massachusetts 02115, United States*

Lanxia Liu − *Departments of Chemistry and Chemical Biology, Chemical Engineering, and Bioengineering, Northeastern University, Boston, Massachusetts 02115, United States;* orcid.org/0000-0002-8153-9678

Jiahe Li − *Department of Bioengineering, Northeastern University, Boston, Massachusetts 02115, United States;* orcid.org/0000-0002-9889-8546

Xin Sun − *Department of Bioengineering, Northeastern University, Boston, Massachusetts 02115, United States*

Mengqi Ren − *Departments of Chemistry and Chemical Biology, Chemical Engineering, and Bioengineering, Northeastern University, Boston, Massachusetts 02115, United States*

Ruoxuan Wang − *Departments of Chemistry and Chemical Biology, Chemical Engineering, and Bioengineering, Northeastern University, Boston, Massachusetts 02115, United States*

Yang Fang − *Departments of Chemistry and Chemical Biology, Chemical Engineering, and Bioengineering, Northeastern University, Boston, Massachusetts 02115, United States*

Jean J. Zhao − *Department of Cancer Biology, Dana-Farber Cancer Institute, Boston, Massachusetts 02115, United States*

Complete contact information is available at: https://pubs.acs.org/10.1021/acs.nanolett.2c00723

Author Contributions

K.Z. and P.C. devised the experiments and wrote the manuscript. D.W., Q.W., and L.L. contributed to the exploratory phase of the study. All authors contributed to material synthesis, purification/characterization, testing, and/or discussion of the results. All authors edited the manuscript.

Funding

Research reported in this publication was supported by the National Cancer Institute (1R01CA251730), the National Institute of General Medical Sciences (1R01GM121612), and the National Science Foundation (DMR award number 2004947). The content is solely the responsibility of the authors and does not necessarily represent the official views of the National Institutes of Health or the National Science Foundation.

Notes

The authors declare no competing financial interest.

■ ACKNOWLEDGMENTS

We thank the institute for Chemical Imaging of Living System at Northeastern University for consultation and imaging support. The images in the table of contents and abstract graphics were created with BioRender.com.

■ ABBREVIATIONS

SNA, spherical nucleic acid; OVA, ovalbumin; APCs, antigen-presenting cells; PRRs, pattern-recognition receptors; TLRs, toll-like receptors; LN, lymph node; VE, vitamin E; daSNA, dual-adjuvanted SNA; DCs, dendritic cells; MHC, major histocompatibility complex

REFERENCES

(1) Schlee, M.; Hartmann, G. Discriminating self from non-self in nucleic acid sensing. *Nature Reviews Immunology* **2016**, *16* (9), 566−580.

(2) Barbalat, R.; Ewald, S. E.; Mouchess, M. L.; Barton, G. M. Nucleic Acid Recognition by the Innate Immune System. *Annu. Rev. Immunol.* **2011**, *29* (1), 185−214.

(3) Rehwinkel, J.; Gack, M. U. RIG-I-like receptors: their regulation and roles in RNA sensing. *Nature Reviews Immunology* **2020**, *20* (9), 537−551.

(4) Hu, H. G.; Li, Y. M. Emerging Adjuvants for Cancer Immunotherapy. *Front Chem.* **2020**, *8*, 601.

(5) Shukla, N. M.; Chan, M.; Hayashi, T.; Carson, D. A.; Cottam, H. B. *Recent advances and perspectives in small-molecule TLR ligands and their modulators*. ACS Publications: 2018.

(6) Wu, J. J.; Zhao, L.; Hu, H. G.; Li, W. H.; Li, Y. M. Agonists and inhibitors of the STING pathway: Potential agents for immunotherapy. *Medicinal research reviews* **2020**, *40* (3), 1117−1141.

(7) Lu, X.; Miao, L.; Gao, W.; Chen, Z.; McHugh, K. J.; Sun, Y.; Tochka, Z.; Tomasic, S.; Sadtler, K.; Hyacinthe, A. Engineered PLGA microparticles for long-term, pulsatile release of STING agonist for cancer immunotherapy. *Science translational medicine* **2020**, *12* (556), 1.

(8) Feng, C.; Li, Y.; Ferdows, B. E.; Patel, D. N.; Ouyang, J.; Tang, Z.; Kong, N.; Chen, E.; Tao, W. Emerging vaccine nanotechnology: From defense against infection to sniping cancer. *Acta Pharmaceutica Sinica B* **2022**, DOI: 10.1016/j.apsb.2021.12.02.

(9) Huang, W.; He, L.; Ouyang, J.; Chen, Q.; Liu, C.; Tao, W.; Chen, T. Triangle-shaped tellurium nanostars potentiate radiotherapy by boosting checkpoint blockade immunotherapy. *Matter* **2020**, *3* (5), 1725−1753.

(10) Le Naour, J.; Zitvogel, L.; Galluzzi, L.; Vacchelli, E.; Kroemer, G. Trial watch: STING agonists in cancer therapy. *Oncoimmunology* **2020**, *9* (1), 1777624.

(11) Vacchelli, E.; Galluzzi, L.; Eggermont, A.; Fridman, W. H.; Galon, J.; Sautès-Fridman, C.; Tartour, E.; Zitvogel, L.; Kroemer, G. Trial watch: FDA-approved Toll-like receptor agonists for cancer therapy. *Oncoimmunology* **2012**, *1* (6), 894−907.

(12) Wang, S.; Qin, L.; Yamankurt, G.; Skakuj, K.; Huang, Z.; Chen, P. C.; Dominguez, D.; Lee, A.; Zhang, B.; Mirkin, C. A. Rational vaccinology with spherical nucleic acids. *Proc. Natl. Acad. Sci. U. S. A.* **2019**, *116* (21), 10473−10481.

(13) Zhu, G.; Zhang, F.; Ni, Q.; Niu, G.; Chen, X. Efficient nanovaccine delivery in cancer immunotherapy. *ACS Nano* **2017**, *11* (3), 2387−2392.

(14) Yamankurt, G.; Berns, E. J.; Xue, A.; Lee, A.; Bagheri, N.; Mrksich, M.; Mirkin, C. A. Exploration of the nanomedicine-design space with high-throughput screening and machine learning. *Nat. Biomed Eng.* **2019**, *3* (4), 318−327.

(15) Liu, S.; Jiang, Q.; Zhao, X.; Zhao, R.; Wang, Y.; Wang, Y.; Liu, J.; Shang, Y.; Zhao, S.; Wu, T.; Zhang, Y.; Nie, G.; Ding, B. A DNA nanodevice-based vaccine for cancer immunotherapy. *Nat. Mater.* **2021**, *20* (3), 421−430.

(16) Xu, J.; Lv, J.; Zhuang, Q.; Yang, Z.; Cao, Z.; Xu, L.; Pei, P.; Wang, C.; Wu, H.; Dong, Z.; Chao, Y.; Wang, C.; Yang, K.; Peng, R.; Cheng, Y.; Liu, Z. A general strategy towards personalized nanovaccines based on fluoropolymers for post-surgical cancer immunotherapy. *Nat. Nanotechnol* **2020**, *15* (12), 1043−1052.

(17) Yu, W.; Sun, J.; Liu, F.; Yu, S.; Xu, Z.; Wang, F.; Liu, X. Enhanced Immunostimulatory Activity of a Cytosine-Phosphate-Guanosine Immunomodulator by the Assembly of Polymer DNA Wires and Spheres. *ACS Appl. Mater. Interfaces* **2020**, *12* (15), 17167−17176.

(18) Gong, N.; Zhang, Y.; Teng, X.; Wang, Y.; Huo, S.; Qing, G.; Ni, Q.; Li, X.; Wang, J.; Ye, X.; Zhang, T.; Chen, S.; Wang, Y.; Yu, J.; Wang, P. C.; Gan, Y.; Zhang, J.; Mitchell, M. J.; Li, J.; Liang, X. J. Proton-driven transformable nanovaccine for cancer immunotherapy. *Nat. Nanotechnol* **2020**, *15* (12), 1053−1064.

(19) Tan, X.; Jia, F.; Wang, P.; Zhang, K. Nucleic acid-based drug delivery strategies. *J. Controlled Release* **2020**, *323*, 240−252.

(20) Ibricevic, A.; Guntsen, S. P.; Zhang, K.; Shrestha, R.; Liu, Y.; Sun, J. Y.; Welch, M. J.; Wooley, K. L.; Brody, S. L. PEGylation of cationic, shell-crosslinked-knedel-like nanoparticles modulates inflammation and enhances cellular uptake in the lung. *Nanomedicine: Nanotechnology, Biology and Medicine* **2013**, *9* (7), 912−922.

(21) Jegerlehner, A.; Wiesel, M.; Dietmeier, K.; Zabel, F.; Gatto, D.; Saudan, P.; Bachmann, M. F. Carrier induced epitopic suppression of antibody responses induced by virus-like particles is a dynamic phenomenon caused by carrier-specific antibodies. *Vaccine* **2010**, *28* (33), 5503−5512.

(22) Tan, X.; Li, B. B.; Lu, X.; Jia, F.; Santori, C.; Menon, P.; Li, H.; Zhang, B.; Zhao, J. J.; Zhang, K. Light-triggered, self-immolative nucleic Acid-drug nanostructures. *J. Am. Chem. Soc.* **2015**, *137* (19), 6112−6115.

(23) Karbach, J.; Neumann, A.; Wahle, C.; Brand, K.; Gnjatic, S.; Jäger, E. Therapeutic administration of a synthetic CpG oligodeoxynucleotide triggers formation of anti-CpG antibodies. *Cancer research* **2012**, *72* (17), 4304−4310.

(24) Klinman, D. M.; Barnhart, K. M.; Conover, J. CpG motifs as immune adjuvants. *Vaccine* **1999**, *17* (1), 19−25.

(25) Tan, X.; Lu, X.; Jia, F.; Liu, X.; Sun, Y.; Logan, J. K.; Zhang, K. Blurring the role of oligonucleotides: spherical nucleic acids as a drug delivery vehicle. *J. Am. Chem. Soc.* **2016**, *138* (34), 10834−10837.

(26) Franchini, A.; Bertuzzi, S.; Tosarelli, C.; Manfreda, G. Vitamin E in viral inactivated vaccines. *Poultry science* **1995**, *74* (4), 666−671.

(27) Bode, C.; Zhao, G.; Steinhagen, F.; Kinjo, T.; Klinman, D. M. CpG DNA as a vaccine adjuvant. *Expert review of vaccines* **2011**, *10* (4), 499−511.

(28) Krieg, A. M. Toll-like receptor 9 (TLR9) agonists in the treatment of cancer. *Oncogene* **2008**, *27* (2), 161−167.

(29) Shirota, H.; Klinman, D. M., CpG Oligodeoxynucleotides as Adjuvants for Clinical Use, *Immunopotentiators in Modern Vaccines*, 2nd ed.; Schijns, V. E. J. C., O'Hagan, D. T., Eds.; Academic Press: 2017, Chapter 9, pp 163−198. DOI: 10.1016/B978-0-12-804019-5.00009-8.

(30) Wang, C.; Ye, Y.; Hu, Q.; Bellotti, A.; Gu, Z. Tailoring biomaterials for cancer immunotherapy: emerging trends and future outlook. *Adv. Mater.* **2017**, *29* (29), 1606036.

(31) Rötzschke, O.; Falk, K.; Stevanovic, S.; Jung, G.; Walden, P.; Rammensee, H. G. Exact prediction of a natural T cell epitope. *European journal of immunology* **1991**, *21* (11), 2891−2894.

(32) McFarland, B. J.; Sant, A. J.; Lybrand, T. P.; Beeson, C. Ovalbumin (323− 339) peptide binds to the major histocompatibility complex class II I-ad protein using two functionally distinct registers. *Biochemistry* **1999**, *38* (50), 16663−16670.

(33) Xia, X.; Mai, J.; Xu, R.; Perez, J. E. T.; Guevara, M. L.; Shen, Q.; Mu, C.; Tung, H.-Y.; Corry, D. B.; Evans, S. E.; et al. Porous silicon microparticle potentiates anti-tumor immunity by enhancing cross-presentation and inducing type I interferon response. *Cell reports* **2015**, *11* (6), 957−966.

(34) Gu, L.; Mooney, D. J. Biomaterials and emerging anticancer therapeutics: engineering the microenvironment. *Nature Reviews Cancer* **2016**, *16* (1), 56−66.

(35) Choi, C. H. J.; Hao, L.; Narayan, S. P.; Auyeung, E.; Mirkin, C. A. Mechanism for the endocytosis of spherical nucleic acid nanoparticle conjugates. *Proc. Natl. Acad. Sci. U. S. A.* **2013**, *110* (19), 7625−7630.

(36) Franchini, A.; Canti, M.; Manfreda, G.; Bertuzzi, S.; Asdrubali, G.; Franciosi, C. Vitamin E as adjuvant in emulsified vaccine for chicks. *Poultry Science* **1991**, *70* (8), 1709−1715.

NOTE ADDED AFTER ASAP PUBLICATION

This paper was published ASAP on May 6, 2022, with an error in the title. The corrected version was reposted on May 10, 2022.

https://doi.org/10.1021/acs.nanolett.2c00723
Nano Lett. XXXX, XXX, XXX−XXX